

1

Modelling Chemical Reactions Using Empirical Force Fields

Tibor Nagy¹ and Markus Meuwly²

¹IMEC, RCNS, Hungarian Academy of Sciences, Budapest, Hungary

²Department of Chemistry, University of Basel, Switzerland

1.1 Introduction

Chemical reactions involve bond-breaking and bond-forming processes and are fundamental in chemistry and the life sciences in general. In many cases, mechanistic aspects of the reactions (“which reaction partners interact at which time with each other”) are of interest. However, many atomistic aspects in bond-breaking and bond-forming processes remain elusive by considering experimental data alone because “the reaction” itself is a transient process. The transition state is unstable and short-lived. Thus, the most interesting regions along a reaction path can not be investigated experimentally in a direct fashion. To shed light on such questions, theoretical and computational work has become invaluable to experimental efforts in understanding particular reaction schemes.

The computational investigation of a chemical or biological system requires models to compute the total energy of the system under investigation. There are two fundamentally different concepts to do that: either by solving the electronic Schrödinger equation, or by assuming a suitably defined empirical potential energy function. The first approach has been refined to a degree that allows one to carry out calculations with “chemical accuracy” – that is, accuracies for relative energies within 1 kcal/mol for the chemically bonded region and less accurately for transition state regions. Most importantly, a quantum chemical calculation makes no assumption on the bonding pattern in the molecule and is ideally suited to answer the question which atoms are bonded to one another for a particular relative arrangement of the atoms. To obtain realistic reaction profiles it is, however, necessary to carry out calculations at a sufficiently high level of theory, particularly in the region of the transition state. Through statistical mechanics and assuming idealized models of molecular motion such as rigid rotor or harmonic oscillator, average internal energies, enthalpies, and by including entropic effects, also free energies can be calculated. However, although such computations are by now standard, they can realistically and routinely only be carried out for systems including several tens of heavy atoms, that is, small systems in the gas phase. This is due to the N^3 scaling of the secular determinants that need to be diagonalized, where N is the number of basis functions.

Alternative approaches to solving the electronic Schrödinger equation have been developed and matured to similar degrees. London’s work on the $H + H_2$ reaction for

which he used a 2×2 valence bond treatment^[1] is an early example for this. Further refined and extended approaches led to the London-Eyring-Polanyi (LEP),^[2] and to the London-Eyring-Polanyi-Sato (LEPS) surfaces.^[3,4] A development that continued the efforts to use valence bond theory to describe multi-state chemical systems, is the diatomics-in-molecules (DIM) theory.^[5] Following a slightly different perspective, Pauling profoundly influenced the theoretical description of chemical reactivity through his work on molecular structure and the nature of the chemical bond.^[6,7] Empirical relationships such as the one between bond length and bond order later became foundations to empirical descriptions of reactivity.^[8,9]

Excluding all electronic effects finally leads to empirical force fields. They were developed with the emphasis on characterizing the structure and dynamics of macromolecules, including peptides and proteins.^[10–17] Thus, their primary application area were sampling and characterizing conformations of larger molecular structures where reorganization of the bonds would not occur. The mathematical form

$$\begin{aligned} V_{\text{bond}} &= \sum K_b (r - r_e)^2 \\ V_{\text{angle}} &= \sum K_\theta (\theta - \theta_e)^2 \\ V_{\text{dihe}} &= \sum K_\phi (1 + \cos(n\phi - \delta)) \end{aligned} \quad (1.1)$$

of empirical force fields is thus not suitable to describe chemical reactions where chemical bonds are broken and formed. Here, K are the force constants associated with the particular type of interaction, r_e and θ_e are equilibrium values, n is the periodicity of the dihedral and δ is the phase which determines the location of the maximum. The sums are carried out over all respective terms. Nonbonded interactions include electrostatic and van der Waals terms, which are

$$\begin{aligned} V_{\text{elstat}} &= \frac{1}{4\pi\epsilon_0} \sum \frac{q_i q_j}{r_{ij}} \\ V_{\text{vdW}} &= \sum \epsilon_{ij} \left[\left(\frac{R_{\text{min},ij}}{r_{ij}} \right)^{12} - 2 \left(\frac{R_{\text{min},ij}}{r_{ij}} \right)^6 \right] \end{aligned} \quad (1.2)$$

where the sums run over all nonbonded atom pairs. q_i and q_j are the partial charges of the atoms i and j involved and ϵ_0 is the vacuum dielectric constant. For the van der Waals terms, the potential energy is expressed as a Lennard-Jones potential with well depth $\epsilon_{ij} = \sqrt{\epsilon_i \epsilon_j}$ and range $R_{\text{min},ij} = (R_{\text{min},i} + R_{\text{min},j})/2$ at the Lennard-Jones minimum. This interaction captures long range dispersion ($\propto -r^{-6}$) and exchange repulsion ($\propto r^{-12}$) where the power of the latter is chosen for convenience. The combination of Eqs. 1.1 and 1.2 constitutes a minimal model for a force field (FF).

An important step to investigate reactions by simulation methods has been the introduction of mixed quantum mechanical/classical mechanics methods (QM/MM).^[18–20] In QM/MM the total system is divided into a (small) reaction region for which the energy is calculated quantum mechanically and a (bulk) environment which is treated with a conventional FF. The majority of applications of QM/MM methods to date use semiempirical (such as AM1, PM3,^[21] SCC-DFTB^[22,23]) or DFT methods. Typically, the QM part contains several tens of atoms. It should also be noted that studies of reactive processes in the condensed phase often employ energy evaluations along the pre-defined progression coordinates,^[21,24] that is, the system is forced to move along a set of more

or less well-suited coordinates. One of the main reasons why *ab initio* QM/MM calculations are not yet used routinely in fully quantitative studies is related to the fact that the energy and force evaluations for the QM region are computationally too expensive to allow meaningful configurational sampling which is required for reliably estimating essential quantities such as free energy changes. Alternatives to QM/MM methods have been developed whereby empirical force fields are used to investigate chemical reactions by combining them in suitable ways. They include RMD (Reactive Molecular Dynamics),^[25–27] EVB (Empirical Valence Bond)^[28] and its variants AVB (Approximate Valence Bond),^[29] and MCMM (Multiconfiguration Molecular Mechanics).^[30]

Force field-based treatments of chemical reactivity start from conventional FFs and employ the diabatic picture of electronic states to define reactant and product states.^[31] From a FF perspective, in a diabatic state the connectivity of the atoms does not change. Low-amplitude vibrations and conformational motion in these states can be efficiently described by conventional FFs. However, they yield very high potential energies, far from their equilibrium geometry, due to their functional form and parametrization. For example, force field evaluation of a chemical bond at its equilibrium geometry for the unbound state, in which the bonded term is replaced by electrostatic and van der Waals interactions, yields a very high energy for the unbound state due to van der Waals repulsion. This large energy difference can be exploited to define a dominant force field which is that with the lowest energy for almost all accessible configurations and makes the energy difference a useful coordinate. Other methods use geometric formulas to switch on and off interactions individually (e.g., ReaxFF). The various methods differ mainly in the choice of switching method and parameters.

The present chapter describes adiabatic reactive molecular dynamics (ARMD),^[27,32] its multi-surface variant (MS-ARMD)^[33–35] and molecular mechanics with proton transfer (MMPT).^[36] All three methods have been developed with the aim to combine the accuracy of quantum methods and the speed of FF simulations such that the processes of interest can be sampled in a statistically meaningful manner. This allows one to determine suitable averages, which can be then compared with experimental data. The chapter first discusses the three methods and briefly highlights similarities and differences to other methods, which are separately discussed in the present volume. Then, topical applications are presented and an outlook laid out future avenues.

1.2 Computational Approaches

In the following chapter the techniques to investigate the energetics and dynamics of chemical reactions based on empirical force fields are discussed. Particular emphasis is put on the methods that allow to follow the rearrangements of atoms along the progression coordinate of a chemical reaction. Excluded from this discussion are nonadiabatic effects and quantum dynamics.

1.3 Molecular Mechanics with Proton Transfer

Molecular Mechanics with Proton Transfer (MMPT) is a parametrized method to follow bond breaking and bond formation between a hydrogen atom (or a proton) and

its donor and acceptor, respectively.^[36] The total interaction energy for the system with coordinates \mathbf{Q} is

$$V(\mathbf{Q}) = V_{\text{MM}}(\mathbf{q}) + V_{\text{PT}}(R, r, \theta), \quad (1.3)$$

where the proton transfer motif D-H-A with donor (D) and acceptor (A) is described by V_{PT} . This contribution is determined from quantum chemical calculations along R (the distance between donor and acceptor atoms), r (the distance between donor and H atom), and θ (the angle between the unit vectors along R and r). The dependence of the total potential energy on the remaining degrees of freedom of the system (\mathbf{q}) is given by a conventional force field V_{MM} . The resulting potential is called Molecular Mechanics with Proton Transfer (MMPT).^[36] In MD simulations with MMPT, the bonding pattern changes upon proton transfer. The algorithm is designed to add, modify, and remove force-field terms, that include bonded and non-bonded interactions, in a smooth and energy conserving fashion by using appropriate switching functions, such as $f_{\text{sw}}(R, r) = 0.5(\tanh(2R(r - R/2)) + 1)$, whenever the migrating H attempts to transfer from donor to acceptor.^[36]

MMPT treats the proton transfer process with its full dimensionality while addressing three important aspects of the problem: speed, accuracy, and versatility. While speed and accuracy are rooted in the QM/MM formulation, the versatility of the approach is exploited by using the morphing potential method.^[37] To this end, it is important to realize that without loss of generality, a wide range of proton transfer processes can be described by three prototype model systems: (a) symmetric single minimum (SSM, optimized structure of the system has equal sharing of the proton), (b) symmetric double-minimum (SDM, optimized structure of the system has unequal sharing of the proton but is symmetric with respect to the transition state), and (c) asymmetric double minimum (ADM, optimized structure of the system has unequal sharing of the proton and is asymmetric with respect to the transition state).^[36] The potential energy surface (PES) of these three model systems, fitted to suitable zeroth order potential energy surfaces (SSM, SDM, or ADM), are morphed into a suitable PES to approximately reproduce important topological features of the target PES by a transformation of the type

$$V_{\text{morph}}(R', r', \theta') = \lambda(R, r, \theta) V_{\text{orig}}(R, r, \theta), \quad (1.4)$$

where λ can either be a constant or a more complicated function of one or more coordinates. The morphing approach not only avoids recomputing a full PES for the proton transfer motif but also reduces the rather laborious task of fitting an entirely new parametrized PES.

1.4 Adiabatic Reactive Molecular Dynamics

In the ARMD^[27,38] simulation method, which is implemented in CHARMM^[39] (since v35b2), at least two parametrized PESs, V_1 for the reactant and V_2 for the product states, are considered. The adiabatic dynamics of the nuclei takes place on the lowest PES while the energy of the higher states is also determined. Whenever the energy of the current state equals that of a higher state, the simulation is restarted from a few fs ($t_s/2$) prior to the detected crossing and during time interval t_s (twice as long), called switching

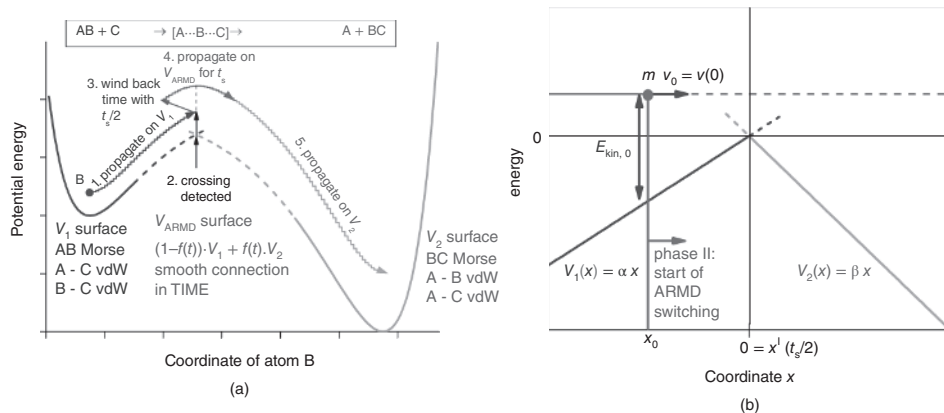


Figure 1.1 (a) The ARMD Method: Schematic Figure of the ARMD Simulation Method for a Collinear Reaction, Where Atom B is Transferred from Donor Atom A to Acceptor Atom C. During crossing the surfaces are switched in time and the Morse bond is replaced by van der Waals (vdW) interactions and vice versa. (b) Simple model for estimating energy violation in ARMD simulations. The system with mass m is approaching from the left on PES $V_1(x)$ (phase I). At $t = 0$ time it is at x_0 with velocity v_0 and kinetic energy $E_{\text{kin},0}$. After crossing is detected at $x = 0$ the time is rewound by $t_s/2$ and the dynamics is re-simulated while $V_1(x)$ is being switched to $V_2(x)$ in t_s (phase II). (See color plate section for the color representation of this figure.)

time, the PESs are mixed in different proportions by multiplying them with a suitable time-dependent smooth switching function $f(t)$ (e.g., a tanh function).^[27,38]

$$V_{\text{ARMD}}(x, t) = (1 - f(t))V_1(x) + f(t)V_2(x). \quad (1.5)$$

At the beginning of the mixing the system is fully in state 1 ($f(0) = 0$), while at the end it is fully in state 2 ($f(t_s) = 1$). The algorithm of ARMD is schematically shown for a collinear atom transfer reaction in Figure 1.1a.

As during surface crossing the ARMD potential energy is explicitly time-dependent, the total energy of the system can not be conserved in a strict sense. For large systems (e.g., proteins in solution) the total energy was found to be conserved to within ≈ 1 kcal/mol which is sufficient for most applications. This allowed successful application of ARMD simulation method to the investigation of rebinding dynamics of NO molecule in myoglobin^[27,38] the dioxygenation of NO into NO_3^- by oxygen-bound truncated hemoglobin.^[40]

However, for highly energetic reactions of small molecules in the gas phase this is not necessarily true. This was the case for vibrationally induced photodissociation of H_2SO_4 .^[35,41] If, however, several crossings between the states involved can take place or the course of the dynamics after the reaction is of interest – for example, for a final state analysis – energy conservation becomes crucial. The magnitude of energy violation ΔE for a simple 1D system (see Figure 1.1b) with effective mass m crossing between two linear potentials $V_1(x) = \alpha x$ and $V_2(x) = \beta x$ using a linear switching function $f(t) = t/t_s$ is:^[34]

$$\Delta E = \frac{\beta(\alpha - \beta)t_s^2}{24m}. \quad (1.6)$$

Hence, exact or nearly exact energy conservation, $\Delta E \approx 0$, can be achieved with ARMD (a) if the steepness of the two PESs along the trajectory during crossing are the same

($\alpha \approx \beta$), (b) if the second surface has a small slope ($\beta \approx 0$) in the crossing region thus accidental cancellation of violations can occur, (c) if the system has a large effective mass, which is often true for biomolecular systems, where both partners are heavy or the reaction is accompanied by the rearrangement of solvation shell involving many solvent molecules, (d) if the switching time is short, however, for $t_s \rightarrow 0$ the connection between the PESs will be unphysically sharp and thus fixed-stepsizes integrators fail to conserve energy.

ARMD involves two or multiple PESs defined by individual sets of force-field parameters. For macromolecular systems, the number of energy terms by which the PESs differ is much smaller compared to the total number of energy terms. Thus, by providing only a smaller number of additional parameters compared to a standard MD simulation, it is possible to describe the difference between the states of interest with limited computational overhead.^[38] Because the FFs for the individual states are separately parametrized, they need to be related to each other by an offset Δ which puts the asymptotic energy differences between the states in the correct order.^[38]

1.5 The Multi-Surface ARMD Method

In the multi-surface (MS) variant of ARMD, the effective potential energy is also a linear combination of n PESs, however with coordinate-dependent weights $w_i(\mathbf{x})$, thereby the total energy is conserved during crossing.

$$V_{\text{MS-ARMD}}(\mathbf{x}) = \sum_{i=1}^n w_i(\mathbf{x}) V_i(\mathbf{x}) \quad (1.7)$$

The $w_i(\mathbf{x})$ are obtained by renormalizing the raw weights $w_{i,0}(\mathbf{x})$, which were calculated by using a simple exponential decay function of the energy difference between surface i and the minimum energy surface with over a characteristic energy scale ΔV (switching parameter).

$$w_i(\mathbf{x}) = \frac{w_{i,0}(\mathbf{x})}{\sum_{i=1}^n w_{i,0}(\mathbf{x})} \quad \text{where } w_{i,0}(\mathbf{x}) = \exp\left(-\frac{V_i(\mathbf{x})}{\Delta V}\right) \quad (1.8)$$

Only those surfaces will have significant weights, whose energy is within a few times of ΔV from the lowest energy surface. The performance of MS-ARMD is demonstrated for crossings of 1D and 2D surfaces in Figure 1.2. A smooth global surface is obtained everywhere, even in regions where more than two surfaces get close in energy.

The CHARMM^[39] implementation (available from v39a2) of MS-ARMD allows adding/removal and reparametrization of terms in any conventional force field, thus it can define new states and can join them into a reactive surface. Morse potentials and generalized Lennard-Jones potential (MIE potential^[42,43]) are also available in the implementation in order to improve the simultaneous description of PES regions close to the equilibrium and the crossing zone. Furthermore, as the energy of each force field is measured from its own global minimum, an additive constant has to be defined for bringing each force field to a common energy scale to reproduce reaction energies.

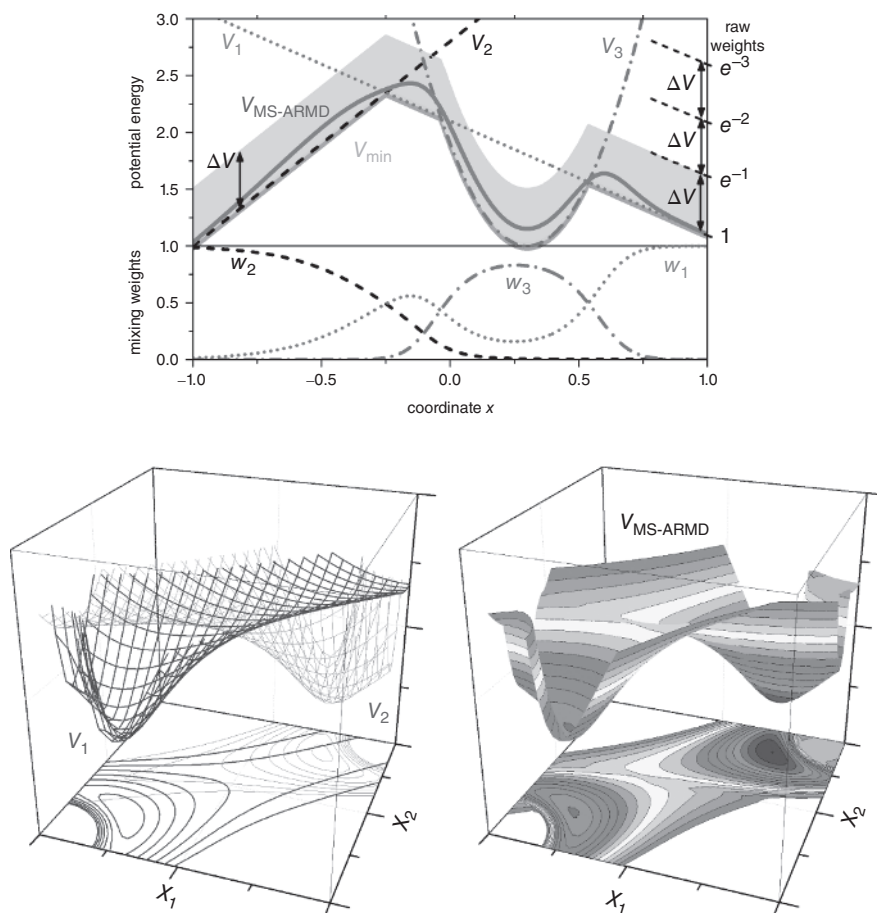


Figure 1.2 MS-ARMD Switching: The MS-ARMD Switching Method Applied in One and Two Dimensions to 3 and 2 Surfaces ($V_{1,2,3}$). The effective surface ($V_{\text{MS-ARMD}}$) always close to the lowest-energy surface (V_{min}), except for regions where other surfaces are within a few times ΔV (here = 0.5) in energy. Here, the algorithm switches smoothly among them by varying their weights ($w_{1,2,3}$; lower left panel of the top figure). (See color plate section for the color representation of this figure.)

Force fields separately optimized for reactant and product states sometimes predict an unrealistic, high-energy crossing point. According to MS-ARMD the transition point between two PESs has a weight of 0.5 from both contributing states. In order to adjust and reshape the barrier region to match energies obtained from electronic structure calculations, products of Gaussian and polynomial functions (GAPOs) ($k = 1, \dots, n_{ij}$) of the energy difference $\Delta V_{ij}(\mathbf{x}) = V_j(\mathbf{x}) - V_i(\mathbf{x})$ can be applied acting between any two surfaces (i and j).

$$\Delta V_{\text{GAPO},k}^{ij}(\mathbf{x}) = \exp\left(-\frac{(\Delta V_{ij}(\mathbf{x}) - V_{ij,k}^0)^2}{2\sigma_{ij,k}^2}\right) \cdot \sum_{i=0}^{m_{ij,k}} a_{ij,kl} (\Delta V_{ij}(\mathbf{x}) - V_{ij,k}^0)^l \quad (1.9)$$

Here, $V_{ij,k}^0$ and $\sigma_{ij,k}$ denote the center and the standard deviation of the Gaussian function, respectively. Whenever the energy difference between the two PESs deviates from $V_{ij,k}^0$ more than a few times of $\sigma_{ij,k}$, the corresponding GAPO functions will be negligible provided that $V_{ij,k}^0$ and $\sigma_{ij,k}$ are small. The global MS-ARMD PES with this extension is a weighted sum of PESs and GAPO functions scaled with the sum of the weights of the two corresponding surfaces:

$$V_{\text{MS-ARMD}}(\mathbf{x}) = \sum_{i=1}^n w_i(\mathbf{x}) V_i(\mathbf{x}) + \sum_{i=1}^{n-1} \sum_{j=i+1}^n [w_i(\mathbf{x}) + w_j(\mathbf{x})] \sum_{k=1}^{n_{ij}} \Delta V_{\text{GAPO},k}^{ij}(\mathbf{x}) \quad (1.10)$$

The CHARMM implementation^[39] of MS-ARMD is a general tool for constructing global potential energy surfaces from empirical force fields for modelling chemical reactions in gas, surface and condensed phases, relevant to homogeneous, heterogeneous and enzymatic catalysis.

1.6 Empirical Valence Bond

One of the established methods to investigate chemical reactions based on empirical force fields is the empirical valence bond (EVB) method.^[28,44] EVB starts from the fact that valence bond states are suitable to distinguish between ionic and covalent resonance forms of a chemical bond which reflects chemical intuition. Since the environment of a chemical reaction primarily interacts through electrostatics with the reactive species, empirical force fields can be used to describe the resonant forms of the reactant and product states. For a bond-breaking reaction $AB \rightarrow A + B$, three resonance forms are introduced: $\psi_1 = AB$, $\psi_2 = A^-B^+$, and $\psi_3 = A^+B^-$. If A is more electronegative than B, resonance structure ψ_3 is largely irrelevant and the process can be described by ψ_1 and ψ_2 .

For a collection of covalent and ionic states, matrix elements for the EVB Hamiltonian have to be determined. They include diagonal elements for the covalent and ionic states, and off-diagonal elements that couple configurations (bonding patterns) that differ by the location of an electron pair. All other off-diagonal matrix elements $H_{ij} = 0$. The justification for this is that such matrix elements are proportional to the square or higher powers of the overlap between atomic orbitals, but they may also be retained.^[28,45] The covalent diagonal matrix elements H_{ii} correspond essentially to an empirical force field, whereas for the ionic diagonal matrix elements the bonded terms are replaced by electrostatic interactions between the charged fragments and the formation energy of A^-B^+ from AB has also to be added. For the two-fragment system AB the matrix elements are $H_{11} = D_e(1 - \exp[-\beta(r - r_e)])^2$ and $H_{22} = \Delta - \frac{e^2}{r} + V_{nb}$ where Δ is the gas-phase formation energy of A^-B^+ from AB at infinite separation, and V_{nb} is the nonbonded interaction potential such that the minimum of $\left(\frac{-e^2}{r} + V_{nb}\right)$ is given by the sums of the ionic radii of A^+ and B^- . In the original version of EVB the off-diagonal element $H_{12} = H_{21}$ is determined through the requirement that the eigenvalues of the Hamiltonian E satisfy the relation $H_{12} = \sqrt{(H_{11} - E)(H_{22} - E)}$ and E is the experimentally determined ground-state bond energy. In a later and slightly more general approach, the off-diagonal

elements are parametrized functions depending on a pre-defined reaction coordinate of the form $H_{ij} = A \exp(-\mu(r - r_0))$.^[44]

The definition of the off-diagonal terms has been a source of considerable discussion in the field, in particular the assumption that upon transfer of the reaction from the gas phase to the solution phase these elements do not change significantly. This assumption has been recently tested.^[44] Alternative forms which also capture the shape and energetics of the potential energy surface around the transition state use generalized Gaussians.^[46] A comparison of different diabatic models has been recently given and provides a notion of the common features and the differences between various approaches.^[47–49] A useful comparison of the similarities and differences between the various methods can be found in the references.^[50] Applications of EVB include enzymatic reactions (for which it was originally developed^[51]), proton transfer processes, and the autodissociation of water.^[52] Furthermore, several extensions have been suggested to the original EVB method allowing its application to a wider class of problems.^[46,53,54]

1.7 ReaxFF

Starting from Pauling's realization that bond order and bond length are related,^[55] a bond energy bond order (BEBO) potential was developed by Johnston and Parr.^[8] It was found that, in addition to the nearly linear relationship between bond order and bond length,^[55] a log-log plot of dissociation energies against bond order is also almost linear. This approach yielded activation energies within ≈ 2 kcal/mol and chemical rates within an order of magnitude for reactants of well-known bond energies. One of the essential assumptions underlying this approach is that – at least for hydrogen-atom transfer reactions – the sum of the bond orders n_1 of the breaking and the newly formed bond n_2 is unity, that is, $n_1 + n_2 = 1$. Or in the words of the authors, that "At all stages of the reaction the formation of the second bond must be 'paying for' the breaking of the first bond."^[8]

A more general method that is based on the concept of bond order and its relationship to bond length and bond energy is ReaxFF.^[9] In this force field, van der Waals and Coulomb terms are included from the beginning and the dissociation and reaction curves are derived from electronic structure calculations. Central to ReaxFF is that the bond order can be calculated from the distance between two atoms. For a CC-bond this expresses the fact that two carbon atoms can be found to form anything in between "no bond" (bond order = 0) to triple bond. From the bond order the bonded energy term E_{bond} is calculated. To correct for over-coordination, a penalty term E_{over} is added to ReaxFF and for under-coordinated atoms additional favorable energy terms E_{under} reflecting resonance energies between π -electrons are introduced. A last, non-standard term usually not present in conventional force fields is the conjugation energy E_{conj} . With these terms, the total potential energy in ReaxFF can be written as

$$E = E_{\text{bond}} + E_{\text{over}} + E_{\text{under}} + E_{\text{conj}} + E_{\text{val}} + E_{\text{pen}} + E_{\text{dihe}} + E_{\text{vdW}} + E_{\text{coul}} \quad (1.11)$$

Here, E_{val} , E_{dihe} , E_{vdw} and E_{coul} are the well-known valence-angle, dihedral, Van der Waals, and electrostatic terms, whereas E_{pen} reproduces the stability of systems with two double bonds sharing an atom in a valence angle. All energy terms and their parametrizations are explained in detail in the references.^[9]

Illustrative applications of ReaxFF range from the study of shock-induced chemistry in high energy materials^[56] to activation and dissociation of H₂ on platinum surfaces^[57] and the oxidation of nanoparticles on aluminum surface.^[58] Using ReaxFF and nonequilibrium MD simulations it was found that depending on the impact velocities cyclic-[CH₂N(NO₂)₃] decomposes into a variety of small molecules on the picosecond time scale or only into NO₂, both of which are consistent with experiments.^[56] Such simulations provide considerable insight into the time dependence of concentration changes of particular species.

1.8 Other Approaches

Multiconfiguration Molecular Mechanics (MCMM): More recently, a procedure that is parametrized entirely with respect to information from ab initio calculations has been put forward. It was termed multiconfiguration molecular mechanics (MCMM). In the light of other existing algorithms MCMM is probably best viewed as a particular variant of EVB.^[47–50] One of the particular features of MCMM is that it uses Shepard interpolation to represent the off-diagonal matrix element H_{12} (see also section on EVB).

Quenching dynamics: Instead of explicitly breaking and forming chemical bonds the possibility has been explored to approximately locate the transition state between the reactant and the product states of a system and subsequently use quenching (down-hill) dynamics to relax the system. Such an approach was employed to investigate the rebinding of CO in myoglobin.^[59] More generally, the approach is reminiscent of using an interpolating Hamiltonian as in the theory of electron transfer.^[60]

1.9 Applications

1.9.1 Protonated Water and Ammonia Dimer

Protonated water dimer has received substantial attention from both experiment^[61–64] and theory.^[65–69] The MMPT potential has been used to investigate the proton transfer dynamics and infrared spectroscopy of protonated water dimer.^[70] The MMPT potential allows to investigate the long-time (several 100 ps) bond-breaking and bond-formation dynamics and how this impacts the vibrational spectroscopy.^[70] MD simulations provide time series of coordinates and dipole moments which are then used to obtain vibrational spectra by Fourier transforming the dipole-dipole autocorrelation functions. For calculating the spectra, the 15 dimensional dipole moment surface of Huang *et al.*^[71] was used. Most experimental line positions, for example the absorptions at 750, 900, 1330, and 1770 cm⁻¹, correspond to features in the calculated infrared spectra. Analyzing power spectra associated with different degrees of freedom, it was established that motion along the O-H* coordinate involved in the O-H*-O asymmetric stretch is coupled to the O-O stretching and the O-H*O and HOH* bending coordinates.^[70] Here, H* is the transferring hydrogen atom. Vibrational excitations estimated from other calculations are well reproduced by the MD simulations with MMPT PES thus validating the approach.^[70] In particular, the MD simulations by Bowman and co-worker^[71] on a

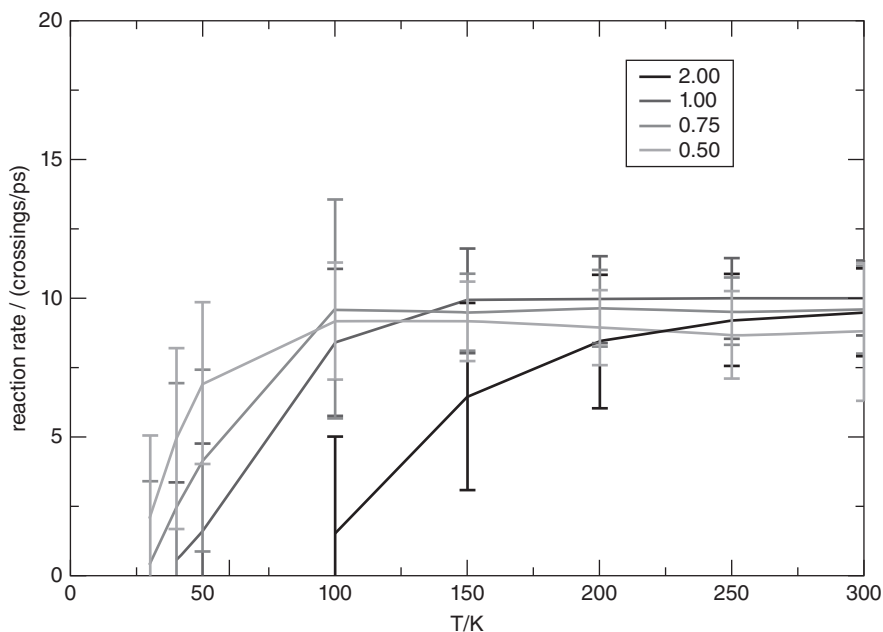


Figure 1.3 Proton Transfer Rates: Rates For Proton Transfer as a Function of T For $\text{NH}_4^+ \cdot \text{NH}_3$ Together with Error Bars. Rates are given for different energy scaling factors λE (proton-transfer barrier heights): $\lambda E = 2.0$ (black), 1.0 (blue), 0.75 (red), and 0.5 (green). For high temperatures the energy scaling has a smaller effect on the barrier than for low temperatures. This also explains why the rates agree within statistical fluctuations for $T \approx 300$ K. The figure is taken from the reference [36]. (See color plate section for the color representation of this figure.)

high-quality 15-dimensional surface find the O-H*-O stretching vibration at 860 cm^{-1} which agrees well with 830 cm^{-1} , calculated with an MMPT potential.

Unlike protonated water dimer, the protonated ammonia dimer represents a symmetric double minima (SDM) potential. Earlier computational studies on protonated ammonia dimer include semiempirical calculations, EVB methods as well as approximate DFT (SCC-DFTB) simulations.^[72–75] Using a SDM potential for the MMPT part and standard force field parameters for the remaining degrees of freedom, MD simulations were carried out at various temperatures between 30 and 300 K. For the SDM potential, no proton transfer was seen below 40 K whereas between 40 K and 150 K a nearly linear increase in the rate is found, beyond which the rate remains constant, see Figure 1.3. To further characterize the rate dependence on the barrier separating the reactant and product, simulations were carried out on morphed PESs where the coordinate-independent morphing parameter λ in Eq. 1.4 was $\lambda = 0.5$, 0.75, and 2.0, respectively. The onset of proton transfer is seen at lower temperatures for potentials with lower barrier, while the high-temperature limit of the proton transfer rate remains unchanged, suggesting that a property common to all surfaces controls the maximum possible rate. Proton transfer probabilities of 8.8 to 10 transfers/ps are found for all barriers investigated. This corresponds to a frequency range associated with the symmetric stretch vibration of the donor and acceptor atoms, which acts as a gating mode.^[36]

1.9.2 Charge Transfer in $N_2 - N_2^+$

In a recent study, the charge-transfer (CT) reaction $N_2^+ + N_2 \rightarrow N_2 + N_2^+$ between Coulomb-crystallized N_2^+ ions at mK temperatures and N_2 molecules from an 8 K beam was investigated by monitoring the change in spinrotational-state population of N_2^+ ions.^[33] The collision of the two interacting partners results in the electronically adiabatic formation of a vibrationally highly-excited $[N-N \cdots N-N]^+$ complex (the well depth is about 29 kcal/mol). After its decay the neutral N_2 leaves the ion trap, whereas the N_2^+ ions remain trapped and were found in rotationally excited states in the experiments.

Interpretation of the experimental findings required computational modelling of the collision process using “quasiclassical trajectory calculations” on an MS-ARMD PES. The PES was fitted accurately (RMSD = 1.4 kcal/mol) to 5565 of UCCSD/cc-pVTZ energies obtained from a global 6D scan. To achieve this accuracy, 24 force fields were needed for describing the three states (bound or complex, 2 unbound: charge-preserving and charge-transferring), which were obtained as follows. Within the complex, 4 connectivities ($N^1N^2-N^3N^4$, $N^1N^2-N^4N^3$, $N^2N^1-N^3N^4$, $N^2N^1-N^4N^3$) can be distinguished. However, at large deformations the complex becomes highly polarized (i.e., either $[N^1N^2](\delta^+) \cdots [N^3N^4](\delta^{++})$ or $[N^1N^2](\delta^{++}) \cdots [N^3N^4](\delta^+)$). Therefore, instead of using a single FF with a symmetric point-charge distribution for a given connectivity, two FFs with opposite polarization are required. Hence, altogether 8 FFs were needed for the 4 complex connectivities and 2 FFs correlating with them were necessary for each unbound state. For the parametrization of individual FFs, Coulomb interaction based on point charges (1-4 interaction in the bound state), Morse and Lennard-Jones potentials were used and within each of the three states, the FFs were related through permutation of the atom indices. The force fields were joined with the MS-ARMD method within the complex (8 FFs), the charge-preserving (2 FFs) and charge-transferring states (2 FFs). During complex formation, the active unbound state was smoothly connected to the bound state with a center of mass ($N_2^+ - N_2$) distance-dependent switching function in the range of 7.09 – 7.56 a_0 . During dissociation, upon reaching separation 7.09 a_0 , the dissociated state with lower potential energy was determined and the bound state was connected to that in the same manner. For an accurate fit of reference energies the flexibility of the global surface was increased by doubling the number of states (and adjustable parameters) to 24.

MS-ARMD simulations showed that the complex is formed up-to large impact parameters of $13a_0$, corresponding to large angular momentum. Upon complex formation (N_4^+) the system accelerates towards the energetically favoured linear arrangement which immediately induces vivid bending vibrations with magnitudes that depend on the impact parameter and the relative orientation of the diatomics. Usually, several rearrangements of the diatomics take place before its decay within 1 – 100 ps. The long average lifetime (10 ps) of the complex provides sufficient time for energy transfer from its overall rotation into bending and torsional vibrational modes, which eventually evolve into enhanced product state rotations after breaking of the central bond.

1.9.3 Vibrationally Induced Photodissociation of Sulfuric Acid

The MS-ARMD method was also applied to the vibrationally induced photodissociation of sulfuric acid (H_2SO_4),^[35,41] which can explain the anomalous enhancement of the

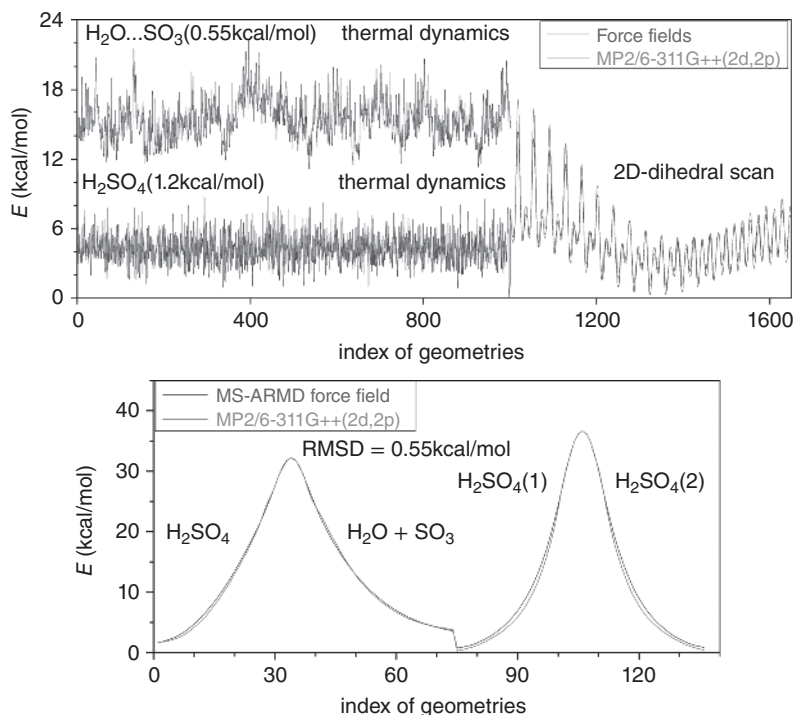


Figure 1.4 Reference MP2 Ab Initio and MS-ARMD Force Field Energies For States H_2SO_4 and $\text{H}_2\text{O} + \text{SO}_3$ and Along the Minimum Energy Paths For Water Elimination and For Intramolecular H-Transfer. (See color plate section for the color representation of this figure.)

polar stratospheric sulfate aerosol layer in springtime.^[76–79] Previous dynamical studies have shown that after significant vibrational excitation of the O-H stretching mode ($\nu_o = 4, 5, 6 \leftarrow 0$ corresponding to 38.6, 47.2 and 55.3 kcal/mol), H_2SO_4 can undergo intramolecular H-transfer ($V_{\text{barr}} = 32.2$ kcal/mol) and $\text{H}_2\text{SO}_4 \rightarrow \text{H}_2\text{O} + \text{SO}_3$ water elimination ($V_{\text{barr}} = 36.6$ kcal/mol).^[41,80]

To explore the ground-state potential energy surface of the system, calculations at MP2 / 6-311G++ (2d,2p) level were carried out for thousands of geometries taken from a 2D rigid dihedral scan of H_2SO_4 and from MD simulations at 300 K using previously developed FFs^[41] for H_2O , SO_3 , H_2SO_4 , and the $\text{H}_2\text{O} \dots \text{SO}_3$ vdW complex. New force fields were constructed using conventional FF terms, Morse and MIE potentials, and were fitted accurately (with RMSDs 0.02, 0.47, 1.23 and 0.55 kcal/mol) to MP2 energies, as shown in Figure 1.4.

Similarly, the minimum energy paths (MEPs) were determined and parameter ΔV and GAPO functions of the global MS-ARMD PES were optimized. Using 3 GAPOs with first-order polynomials for the H_2O elimination, and 2 GAPOs with second-order polynomials for the H-transfer reactions an accurate fit (RMSD = 0.55 kcal/mol) could be achieved, which is also shown in Figure 1.4.

After intramolecular H-transfer a sulfuric acid with different connectivity is obtained. Similarly, altogether, 8 H_2SO_4 and 4 $\text{H}_2\text{O} + \text{SO}_3$ states can be derived as both H atoms can be transferred and water elimination can involve any of the O atoms. Both sets

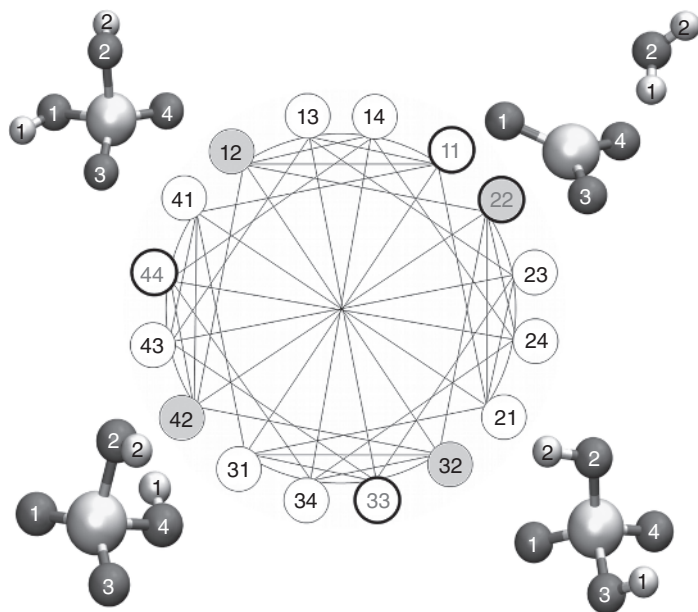


Figure 1.5 Reaction Network For H_2SO_4 : The Network of States (Circles) and Possible Reactions Between Them (Edges) For H_2SO_4 Represented as a Symmetric Graph. States labelled by two-digit numbers denoting the O indices of atoms to which atoms H1 and H2 bind. The four thick-line circles with identical digits indicates $\text{H}_2\text{O} + \text{SO}_3$ states, whereas the remaining 8 are H_2SO_4 states. Four states highlighted in green and given as a ball-and-stick representation were observed in a typical trajectory ($12 \rightarrow 32 \rightarrow 12 \rightarrow 42 \rightarrow 22$) showing three subsequent intramolecular H-transfers and water elimination at the end. (See color plate section for the color representation of this figure.)

of states are chemically equivalent to one another, therefore their FF and GAPO parametrizations need to be the same, but with permuted indices. The network of 16 states and possible 24-24 H-transfer and H_2O -elimination reactions between them can be represented as a graph (Figure 1.5).

Vibrational excitation by 4-6 quanta of thermalized (300 K) H_2SO_4 molecules was invoked by scaling the velocities along the OH-local mode.^[41,81] Then free dynamics was followed for several thousand trajectories until water elimination took place or at most for 1 ns. While several H-transfers and the final dissociation occurred, the total energy was conserved, which served as the validation of the MS-ARMD implementation in CHARMM.

Compared to previous studies,^[41,81] the MS-ARMD simulations were based on a more accurate PES which also enabled the competing intramolecular H-transfer process^[35] and thus lead to quite different lifetime distributions. The MS-ARMD description also allowed the analysis of products states, which showed distinct excitations that can help experimentalists to establish the vibrationally induced decay mechanism proposed by Vaida *et al.*^[79] Furthermore, kinetic analysis of the lifetime distributions lead to the conclusion that vibrationally induced photolysis rate drops significantly with decreasing altitude in the stratosphere due to the competing quenching process.

1.9.4 Proton Transfer in Malonaldehyde and Acetyl-Acetone

Proton Transfer in Malonaldehyde: Malonaldehyde (MA) has long served as a typical hydrogen transfer system to test and validate various computational approaches. Experimentally, the ground state tunneling splitting was determined to be 21.58314 cm^{-1} by different experiments with very high accuracy.^[82,83] Infrared spectra of MA have also been recorded at high resolution.^[84–87]

MMPT simulations with a generalization of the method to nonlinear H-bonds were carried out in order to determine the tunneling splittings for H- and D-transfer and to locate the position of the proton-transfer band in the infrared.^[88] Building on a harmonic bath averaged Hamiltonian (HBA) the effective reduced mass was chosen such as to reproduce the tunneling splitting for H-transfer. The effective reduced mass differs from the mass of the transferring hydrogen atom due to kinetic coupling in the system.^[88] However, the effective mass of the deuterated species is then determined by usual isotopic mass ratios which allows to validate the model because no new parameters are required. The computed tunneling splittings of 22.0 cm^{-1} and 2.9 cm^{-1} compare favourably with the experimentally determined ones which are 21.583 cm^{-1} and 2.915 cm^{-1} , respectively.^[82,83,89] The proton transfer mode exhibits a large red shifts relative to usual OH-stretching vibrations and is found at 1543 cm^{-1} .

Building on this MMPT potential a quantum mechanical treatment of the kinetic isotope effect (KIE) in MA was attempted. The KIE relates the rate constants for hydrogen and deuterium transfer via $\text{KIE} = k_{\text{H}}/k_{\text{D}}$. The KIE for the intramolecular hydrogen transfer in MA has not been determined experimentally. Combining a fully dimensional and validated PES^[88] based on molecular mechanics with proton transfer (MMPT)^[36] with quantum instanton (QI) path integral Monte Carlo (PIMC) simulation the primary H/D KIE on the intramolecular proton transfer in MA was found to be 5.2 ± 0.4 at room temperature.^[90] For higher temperatures, the KIE tends to 1, as required. Periodic orbit theory-based tunneling rate estimates and detailed comparisons with conventional transition state theory (CTST) at various levels suggest that the KIE in MA is largely determined by zero-point energy effects and that tunneling plays a minor role.

Proton Transfer in Acetyl-Acetone: Related to MA is acetyl-acetone (AcAc) but the proton transfer dynamics is far less well characterized. Although infrared and microwave spectra have been recorded, the symmetry of the ground state structure is still debated.^[91–96] Recent infrared experiments combined with atomistic simulations using an MMPT force field and quantum chemical calculations have considered the dynamics of the hydrogen transfer motion in AcAc.^[97] The morphed potential exhibits a barrier of 2.35 kcal/mol and was used in finite-temperature MD simulations from which the IR spectra was determined.

Experimentally, the fundamental OH-stretching band is observed as a broad band red-shifted relative to usual OH-stretching transitions by several hundred wavenumbers.^[97] The IR and power spectra from the MMPT simulations reproduce most experimentally recorded features and clearly assign the ν_{OH} proton transfer (PT) mode to the band experimentally observed in the $2000 - 3300 \text{ cm}^{-1}$ region. The location of this band was found to sensitively depend on the barrier for PT. Simulations with varying barrier heights and comparison of the power spectra with the experimental IR spectrum yield a barrier of $\approx 2.5 \text{ kcal/mol}$. This compares with a value of 3.2 kcal/mol from CCSD(T)

calculations and suggests that such an approach is meaningful to determine approximate barrier heights for proton transfer reactions which is difficult if not impossible from experiment alone.

1.9.5 Rebinding Dynamics in MbNO

Myoglobin, besides being an important model system for understanding the relation between structure and function of proteins, has also been of interest due to its ligand binding properties. In particular, the migration pathways and rebinding dynamics of diatomic ligands such as O₂, NO, and CO inside the protein matrix have been studied by both experimental and computational methods. While rebinding of CO is nonexponential at low temperature, it becomes exponential at high temperature with a time scale of 100 ns, rebinding of NO is nonexponential at all temperature, with time constants of the order of tens of picoseconds.^[98,99]

The rebinding dynamics of MbNO was studied employing the ARMD method. To this end, two force fields were prepared corresponding to the bound and dissociated states, differing in a number of energy terms. The dissociating Fe-N bond was described by a Morse potential to describe the anharmonic nature of the bond. Multiple trajectory simulations were carried out for $\Delta = 60, 65,$ and 70 kcal/mol.^[38]

To visualize the crossing seam all observed crossing geometries are projected onto a plane containing the Fe-N distance and the angle formed by Fe and the ligand NO. The most probable iron-ligand distance lies around 3 \AA .^[38] The distribution is rather wide along the bond angle coordinate and the crossing seam is found to be rather insensitive towards the value of Δ , see Figure 1.6.

The time series of fraction of trajectories without showing crossing provides information about the kinetics of rebinding. The choice of Δ is found to have a substantial effect on the time constant associated with the rebinding reaction, although for all values of Δ the rebinding remains nonexponential. For $\Delta = 65$ kcal/mol, the time constants are found to be 3.6 and 373 ps^[38] compared to the experimental (from ultrafast IR spectroscopy) value of 5.3 and 133 ps.^[99,100] While the fast rebinding component is well reproduced by ARMD, the agreement for the slower component is poor which arises due to an insufficient sampling of the slow time scale by ARMD.

1.9.6 NO Detoxification Reaction in Truncated Hemoglobin (trHbN)

Truncated hemoglobin is a recently discovered heme protein found in plants, bacteria, and lower eukaryots. The trHbN of *Mycobacterium tuberculosis* has been proposed to play an important role in the survival of the bacteria causing tuberculosis in host cells by converting toxic NO to harmless NO₃⁻. The large second-order rate constant of $7.5 \times 10^8 \text{ M}^{-1} \text{ s}^{-1}$ has been attributed to the existence of a continuous tunnel inside the protein which assists ligand migration.^[101,102] However, an atomistic understanding about the mechanism of the detoxification reaction had remained illusive.

ARMD was used to shed light on the reaction by dividing the overall reaction into following four steps:^[103]



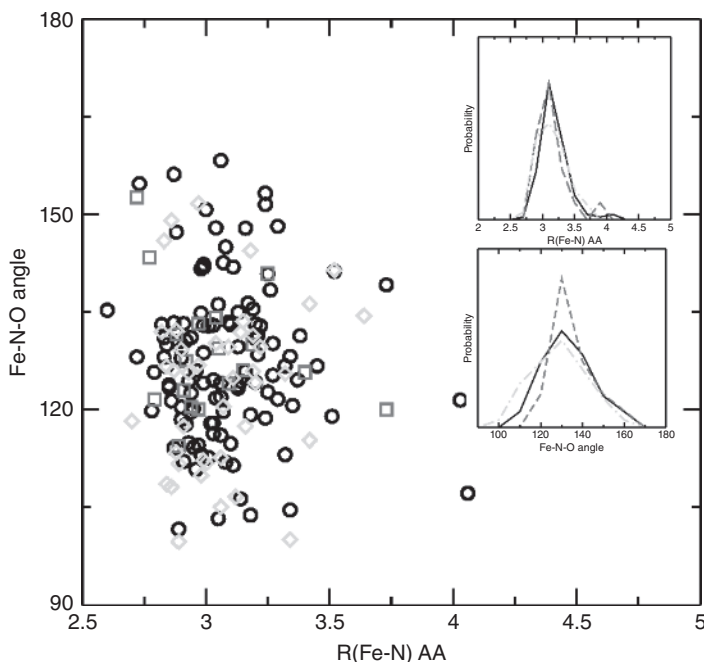


Figure 1.6 Crossing Seam For NO-Rebinding: The Crossing Geometries of NO Rebinding to Mb For Three Different Values of Δ (Red Squares $\Delta = 60$, Black Circles $\Delta = 65$, and Green Diamonds $\Delta = 70$ kcal/mol) Projected Onto the Distance Between Iron and the Nitrogen of the Ligand R_{FeN} and the Angle Between Iron and the NO Ligand θ_{FeNO} . The insets show the distributions of crossing points along the R_{FeN} (upper) and θ_{FeNO} (lower) coordinates. For the insets, broken, solid, and dash-dotted lines denote $\Delta = 60, 65,$ and 70 kcal/mol, respectively. The figure is taken from Reference [38]. (See color plate section for the color representation of this figure.)

The right-hand side column of the above reaction steps indicates the bond broken/formed bond in the reaction step. First, oxy-trHbN reacts with free NO and forms a peroxy-nitrite intermediate, which then undergoes homolytic fission. This is followed by the rebinding of free NO_2 to the oxo-ferryl species to form the heme-bound nitrate complex, which then undergoes heme-ligand dissociation, resulting in free NO_3^- and penta-coordinated heme.

The force field parameters associated with the reactants and products of each of the reaction steps are obtained from ab initio calculations. Each of the reaction steps was then studied by running multiple ARMD trajectories with a range of Δ values.^[40] For reaction steps I, III, and IV, the ARMD simulations yielded rate constants on the picosecond time scale. The choice of the free parameter Δ had only limited effects on the reaction rate.

For step II, however, no reactive events even on the nanosecond time scale were found.^[40] From DFT calculations it is known that this step involves a barrier of 6.7 kcal/mol.^[104] Umbrella sampling simulations with ARMD yielded a barrier of 12-15 kcal/mol which corresponds to timescales on the order of micro- to milliseconds. Since experimentally, the overall reaction is on the picosecond time scale, it is unlikely that the reaction occurs via step II. This proposition is in line with the lack of experimental detection of free NO_2 radical in several studies which propose an alternative mechanism where peroxy-nitrite intermediate rearranges to nitrate complex.^[105,106]

To further corroborate this, ARMD simulations for the rearrangement reaction were carried out and found this process to occur within picoseconds, explaining the fast overall detoxification reaction.^[40]

1.9.7 Outlook

This outlook summarizes the methods presented in this chapter and describes potential improvements in investigating reactions using force fields.

The common feature of the EVB, ARMD and MS-ARMD methods is that they combining force fields by giving preference to the lowest energy surface, thus inherently the energy difference between the surfaces serves as a reaction coordinate. In EVB, the smooth switching is carried out by formally carrying out an adiabaticization of diabatic PESs, which is controlled by couplings between the states. These coupling terms have to decay when moving away from the dividing surface, which is assumed to depend on a predefined geometric reaction coordinate, whose determination, however, in complex reactions is not straightforward. Contrary to that, smooth switching in ARMD and MS-ARMD is carried out by time- and energy-dependent switching functions controlled by the switching time t_s or a switching parameter ΔV , respectively. These latter switching variables are one dimensional thus naturally serve as a reaction coordinate, whereas in the case of geometrical switching variables the determination of reaction coordinate is neither straightforward nor unambiguous. Furthermore, the potential energy and its gradient are analytic functions of the individual force field energies, whereas in EVB the matrix diagonalization allows efficient analytic evaluation only for a small number of surfaces due to the diagonalization involved.

Due to the explicit time-dependence of the ARMD Hamiltonian, the ARMD crossing is inherently a dynamical method and this is also the reason for violations of energy conservation observed during crossing in gas-phase reactions of highly-excited small molecules. On the contrary, in the MS-ARMD and EVB methods the PES is stationary and thus they can be used in *NVE* simulations. The ARMD method cannot describe crossings in regions properly where more than two surfaces are close in energy, whereas the MS-ARMD technique can be applied to the simultaneous switching among multiple PESs. Finally, in MS-ARMD, the height and the shape of the crossing region can be adjusted in a flexible manner, which makes it very similar in functionality to EVB, but without the need of referring to any geometrical reaction coordinate. This extension makes the CHARMM implementation of MS-ARMD method^[39] comparable to QM/MM methods in capability of modelling complex chemical reaction in gas, surface, and condensed phases albeit at the accelerated speed of a conventional force field simulation and with the only added effort of parametrization.

Future improvements of the ARMD and MS-ARMD methods include the more routine development of accurate force field parametrizations which still poses an obstacle to a more routine use of such approaches in all areas of chemistry and biophysics. For ARMD, which requires an asymptotic offset Δ between the states, an improvement could be achieved by making this parameter coordinate-dependent. On the other hand, this would introduce one or several geometric progression coordinates whose definition may be difficult. Nevertheless, a recent study of nitric oxide rebinding to Mb found that indeed, Δ is not constant but depends on the iron-out-of-plane position in this particular situation.^[107] Hence, a better reaction energetics and a more realistic modelling of the ligand-(re)binding dynamics is obtained from such improvements.

The current implementation of MS-ARMD requires the separate definition and evaluation of force fields for each possible product connectivity. This means several possibilities in solvent-phase or surface-phase simulations where the reaction can take place with any of the solvent molecules or at any of the surface sites. Even though the common part of all force fields are evaluated only once, the calculation and even the enumeration of all cases is unnecessary. In future developments, this will be constrained to a small number of momentary physically sensible connectivities by an automatic geometrical preselection.

At present, MMPT supports the transfer of one proton/hydrogen atom between one designated donor/acceptor pair. Combining this with the MS-ARMD philosophy will allow one to automatically determine the most probable H-bonding pattern and the dynamics involving them, which would bring the method much closer to QM/MM simulations.

Force field-based approaches to study chemical reactions is becoming more widespread as the functionalities are made available in commonly used atomistic simulation programs. They allow to study chemical reactivity on time scales relevant to the real processes and provide insight complementary to experiment provided that the underlying force fields are accurate. The fitting of reactive force fields remains a challenge but generalizing and simplifying this step will make such approaches valuable additions to the toolbox of computational and experimental chemists interested in chemical reactivity.

Acknowledgements

This work was supported by the Swiss National Science Foundation through grants 200021-117810, the NCCR MUST, and the University of Basel, which is gratefully acknowledged. We thank all coworkers mentioned in the references for their contributions to the methods and their applications discussed in the present work.

References

- 1 London, F.Z. (1929) Quantum mechanical interpretation of the process of activation. *Zeitschrift für Elektrochemie*, **35**, 552–555.
- 2 Eyring, H. and Polanyi, M.Z. (1931) Concerning simple gas reactions. *Zeitschrift für Physikalische Chemie. Abteilung B*, **12**, 279–311.
- 3 Sato, S. (1955) On a new method of drawing the potential energy surface. *Journal of Chemical Physics*, **23**, 592–593.
- 4 Sato, S. (1955) Potential energy surface of the system of three atoms. *Journal of Chemical Physics*, **23**, 2465–2466.
- 5 Ellison, F.O. (1963) A method of diatomics in molecules. 1. General theory and application to H₂O. *Journal of the American Chemical Society*, **85**, 3540–3544.
- 6 Pauling, L. (1960) *The nature of the chemical bond*, Cornell University Press, Ithaca, NY.
- 7 Pauling, L. (1932) The nature of the chemical bond. IV. The energy of single bonds and the relative electronegativity of atoms. *Journal of the American Chemical Society*, **54**, 3570–3582.

- 8 Johnston, H.S. and Parr, C. (1963) Activation energies from bond energies. I. Hydrogen transfer reactions. *Journal of the American Chemical Society*, **85**, 2544–2551.
- 9 van Duin, A.C.T., Dasgupta, S., Lorant, F. and Goddard, W.A. III, (2001) A reactive force field for hydrocarbons. *Journal of Physical Chemistry A*, **105**, 9396–9409.
- 10 Lifson, S. and Warshel, A. (1968) Consistent force field for calculations of conformations vibrational spectra and enthalpies of cycloalkane and n-alkane molecules. *Journal of Chemical Physics*, **49**, 5116–5129.
- 11 Levitt, M. and Lifson, S. (1969) Refinement of protein conformations using a macromolecular energy minimization procedure. *Journal of Molecular Biology*, **46**, 269–279.
- 12 Hwang, M.J., Stockfisch, T.P. and Hagler, A.T. (1994) Derivation of class II force fields: 2. Derivation and characterization of a class II force field, CFF93, for the alkyl functional group and alkane molecules. *Journal of the American Chemical Society*, **116**, 2515–2525.
- 13 Maple, J.R., Hwang, M.J., Stockfisch, T.P. *et al.* (1994) Derivation of class-II force-fields. 1. Methodology and quantum force-field for the alkyl functional-group and alkane molecules. *Journal of Computational Chemistry*, **15**, 162–182.
- 14 Brooks, B., Brucoleri, R., Olafson, B. *et al.* (1983) CHARMM: A program for macromolecular energy, minimization, and dynamics calculations. *Journal of Computational Chemistry*, **4**, 18–217.
- 15 Weiner, S.J., Kollman, P.A., Case, D.A. *et al.* (1984) A new force-field for molecular mechanical simulation of nucleic-acids and proteins. *Journal of the American Chemical Society*, **106**, 765–784.
- 16 Jorgensen, W.L. and Tirado-Rives, J. (1988) The OPLS potential functions for proteins-energy minimizations for crystals of cyclic-peptides and crambin. *Journal of the American Chemical Society*, **110**, 1657–1666.
- 17 Hermans, J., Berendsen, H.J.C., van Gunsteren, W.F. and Postma, J.P.M. (1984) A consistent empirical potential for water-protein interactions. *Biopolymers*, **23**, 1.
- 18 Warshel, A. and Levitt, M. (1976) Theoretical studies of enzymic reactions: Dielectric, electrostatic and steric stabilization of the carbonium ion in the reaction of lysozyme. *Journal of Molecular Biology*, **103**, 227–249.
- 19 Alagona, G., Ghio, C. and Kollman, P. (1986) A simple-model for the effect of glu165- \rightarrow asp165 mutation on the rate of catalysis in triose phosphate isomerase. *Journal of Molecular Biology*, **191**, 23–27.
- 20 Bash, P.A., Field, M.J. and Karplus, M. (1987) Free-energy perturbation method for chemical-reactions in the condensed phase – a dynamical approach based on a combined quantum and molecular mechanics potential. *Journal of the American Chemical Society*, **109**, 8092–8094.
- 21 Claeysens, F., Ranaghan, K.E., Manby, F.R. *et al.* (2005) Multiple high-level QM/MM reaction paths demonstrate transition-state stabilization in chorismate mutase: correlation of barrier height with transition-state stabilization. *Chemical Communications*, **40**, 5068–5070.
- 22 Zhou, H.Y., Tajkhorshid, E., Frauenheim, T. *et al.* (2002) Performance of the AM1, PM3, and SCC-DFTB methods in the study of conjugated Schiff base molecules. *Chemical Physics*, **277**, 91–103.

- 23 König, P.H., Ghosh, N., Hoffmann, M. *et al.* (2006) Toward theoretical analysis of long-range proton transfer kinetics in biomolecular pumps. *Journal of Physical Chemistry A*, **110**, 548–563.
- 24 Cui, Q., Elstner, T. and Karplus, M. (2003) A theoretical analysis of the proton and hydride transfer in liver alcohol dehydrogenase (LADH). *Journal of Physical Chemistry B*, **106**, 2721–2740.
- 25 Li, H., Elber, R. and Straub, J.E. (1993) Molecular-dynamics simulation of NO recombination to myoglobin mutants. *Journal of Biological Chemistry*, **268**, 17908–17916.
- 26 Meuwly, M., Becker, O.M., Stote, R. and Karplus, M. (2002) NO rebinding to myoglobin: A reactive molecular dynamics study. *Biophysical Chemistry*, **98**, 183–207.
- 27 Nutt, D.R. and Meuwly, M. (2006) Studying reactive processes with classical dynamics: Rebinding dynamics in MbNO. *Biophysical Journal*, **90**, 1191–1201.
- 28 Warshel, A. and Weiss, R.M. (1980) An empirical valence bond approach for comparing reactions in solutions and in enzymes. *Journal of the American Chemical Society*, **102**, 6218–6226.
- 29 Grochowski, P., Lesyng, B., Bala, P. and McCammon, J.A. (1996) Density functional based parametrization of a valence bond method and its applications in quantum-classical molecular dynamics simulations of enzymatic reactions. *International Journal of Quantum Chemistry*, **60**, 1143–1164.
- 30 Kim, Y., Corchado, J.C., Villa, J. *et al.* (2000) Multiconfiguration molecular mechanics algorithm for potential energy surfaces of chemical reactions. *Journal of Chemical Physics*, **112**, 2718–2735.
- 31 Van Voorhis, T., Kowalczyk, T., Kaduk, B. *et al.* (2010) The diabatic picture of electron transfer, reaction barriers, and molecular dynamics. *Annual Review of Physical Chemistry*, **61**, 149–170.
- 32 Dayal, P., Weyand, S.A., McNeish, J. and Mosey, N.J. (2011) Temporal quantum mechanics/molecular mechanics: Extending the time scales accessible in molecular dynamics simulations of reactions. *Chemical Physics Letters*, **516**, 263–267.
- 33 Tong, X., Nagy, T., Reyes, J.Y. *et al.* (2012) State-selected ionmolecule reactions with Coulomb-crystallized molecular ions in traps. *Chemical Physics Letters*, **547**, 1–8.
- 34 Nagy, T., Yosa Reyes, J. and Meuwly, M. (2014) Multisurface adiabatic reactive molecular dynamics. *Journal of Chemical Theory and Computation*, **10**, 1366–1375.
- 35 Yosa Reyes, J., Nagy, T. and Meuwly, M. (2014) Competitive reaction pathways in vibrationally induced photodissociation of H₂SO₄. *Physical Chemistry Chemical Physics*, **16**, 18533–18544.
- 36 Lammers, S., Lutz, S. and Meuwly, M. (2008) Reactive force fields for proton transfer dynamics. *Journal of Computational Chemistry*, **29**, 1048–1063.
- 37 Meuwly, M. and Huston, J. (1999) Morphing ab initio potentials: A systematic study of Ne-HF. *Journal of Chemical Physics*, **110**, 8338–8347.
- 38 Danielsson, J. and Meuwly, M. (2008) Atomistic simulation of adiabatic reactive processes based on multi-state potential energy surfaces. *Journal of Chemical Theory and Computation*, **4**, 1083–1093.
- 39 Brooks, B.R. *et al.* (2009) CHARMM: The biomolecular simulation program. *Journal of Computational Chemistry*, **30**, 1545–1614.

- 40 Mishra, S. and Meuwly, M. (2010) Atomistic simulation of NO dioxygenation in Group I truncated hemoglobin. *Journal of the American Chemical Society*, **132**, 2968.
- 41 Yosa, J. and Meuwly, M. (2011) Vibrationally induced dissociation of sulfuric acid (H_2SO_4). *Journal of Physical Chemistry A*, **115**, 14350–14360.
- 42 Mie, G. (1903) Zur kinetischen Theorie der einatomigen Körper. *Annals of Physics*, **11**, 657–697.
- 43 Kramer, C., Gedeck, P. and Meuwly, M. (2013) Multipole-based force fields from interaction energies and the need for jointly refitting all intermolecular parameters. *Journal of Chemical Theory and Computation*, **9** (3), 1499–1511.
- 44 Hong, G., Rosta, E. and Warshel, A. (2006) Using the constrained DFT approach in generating diabatic surfaces and off diagonal empirical valence bond terms for modeling reactions in condensed phases. *Journal of Physical Chemistry B*, **110**, 19570–19574.
- 45 Coulson, C.A. and Danielsson, U. (1954) Ionic and covalent contributions to the hydrogen bond. *Arkiv för Fysik*, **8**, 239–244.
- 46 Chang, Y.-T. and Miller, W.H. (1990) An empirical valence bond model for constructing global potential energy surfaces for chemical reactions of polyatomic molecular systems. *Journal of Physical Chemistry*, **94**, 5884–5888.
- 47 Valero, R., Song, L., Gao, J. and Truhlar, D.G. (2009) Perspective on diabatic models of chemical reactivity as illustrated by the gas-phase $\text{S}_{\text{N}}2$ reaction of acetate ion with 1,2-dichloroethane. *Journal of Chemical Theory and Computation*, **5**, 1–22.
- 48 Valero, R., Song, L., Gao, J. and Truhlar, D.G. (2009) Erratum: Perspective on diabatic models of chemical reactivity as illustrated by the gas-phase $\text{S}_{\text{N}}2$ reaction of acetate ion with 1,2-dichloroethane. *Journal of Chemical Theory and Computation*, **5**, 2191–2191.
- 49 Kamerlin, S.C.L., Cao, J., Rosta, E. and Warshel, A. (2009) On unjustifiably misrepresenting the EVB approach while simultaneously adopting it. *Journal of Physical Chemistry B*, **113**, 10905–10915.
- 50 Florian, J. (2002) Comments on molecular mechanics for chemical reactions. *Journal of Physical Chemistry A*, **106**, 5046–5047.
- 51 Warshel, A. (1984) Dynamics of enzymatic reactions. *Proceedings of the National Academy of Sciences USA*, **81**, 444–448.
- 52 Strajbl, M., Hong, G. and Warshel, A. (2002) Ab initio QM/MM simulation with proper sampling: "First principle" calculations of the free energy of the autodissociation of water in aqueous solution. *Journal of Physical Chemistry B*, **106**, 13333–13343.
- 53 Schmitt, U. and Voth, G. (1998) Multistate empirical valence bond model for proton transport in water. *Journal of Physical Chemistry B*, **102**, 5547–5551.
- 54 Schlegel, H.B. and Sonnenberg, J.L. (2006) Empirical valence-bond models for reactive potential energy surfaces using distributed Gaussians. *Journal of Chemical Theory and Computation*, **2**, 905–911.
- 55 Pauling, L. (1947) Atomic radii and interatomic distances in metals. *Journal of the American Chemical Society*, **69**, 542–553.
- 56 Strachan, A., van Duin, A.C.T., Chakraborty, D. *et al.* (2003) Shock waves in high-energy materials: The initial chemical events in nitramine RDX. *Physical Review Letters*, **91**, 098301–1.

- 57 Ludwig, J., Vlachos, D.G., van Duin, A.C.T. and Goddard, W.A. III, (2006) Dynamics of the dissociation of hydrogen on stepped platinum surfaces using the ReaxFF reactive force field. *Journal of Physical Chemistry B*, **110**, 4274–4282.
- 58 Vashishta, P., Kalia, R.K. and Nakano, A. (2006) Multimillion atom simulations of dynamics of oxidation of an aluminum nanoparticle and nanoindentation on ceramics. *Journal of Physical Chemistry B*, **110**, 3727–3733.
- 59 Zheng, D., Makarov, V. and Wolynes, P.G. (1996) Statistical survey of transition states and conformational substates of the sperm whale myoglobin-CO reaction system. *Journal of the American Chemical Society*, **118**, 2818–2824.
- 60 Marcus, R.A. (1993) Electron-transfer reactions in chemistry – theory and experiment. *Angewandte Chemie International Edition*, **32**, 1111–1121.
- 61 Asmis, K.R., Pivonka, N.L., Santambrogio, G. *et al.* (2003) Gas phase infrared spectrum of the protonated water dimer. *Science*, **299**, 1375–1377.
- 62 Fridgen, T.D., McMahon, G.B., MacAleese, L. *et al.* (2004) Infrared spectrum of the protonated water dimer in the gas phase. *Journal of Physical Chemistry A*, **108**, 9008–9010.
- 63 Moore, D.R., Oomens, J., van der Meer, L. *et al.* (2004) Probing the vibrations of shared, OH⁺O⁻-bound protons in the gas phase. *Computer Physics Communications*, **5**, 740–743.
- 64 Hammer, N.I., Diken, E.G., Roscioli, J.R. *et al.* (2005) The vibrational predissociation spectra of the H₅O₂⁺·RG_n (RG = Ar, Ne) clusters: Correlation of the solvent perturbations in the free OH and shared proton transitions of the Zundel ion. *Journal of Chemical Physics*, **122**, 244301.
- 65 Dai, J., Bacic, Z., Huang, X. *et al.* (2003) A theoretical study of vibrational mode coupling in H₅O₂⁺. *Journal of Chemical Physics*, **119**, 6571–6580.
- 66 Kaledin, M., Kaledin, A.L. and Bowman, J.M. (2006) Vibrational analysis of the H₅O₂⁺ infrared spectrum using molecular and driven molecular dynamics. *Journal of Physical Chemistry A*, **110**, 2933–2939.
- 67 Lobaugh, J. and Voth, G.A. (1996) The quantum dynamics of an excess proton in water. *Journal of Chemical Physics*, **104**, 2056–2059.
- 68 Cho, H.M. and Singer, S.J. (2004) Correlation function quantum Monte Carlo study of the excited vibrational states of H₅O₂⁺. *Journal of Physical Chemistry A*, **108**, 8691–8702.
- 69 Sauer, J. and Doebler, J. (2005) Gas-phase infrared spectrum of the protonated water dimer: molecular dynamics simulation and accuracy of the potential energy surface. *Computer Physics Communications*, **6**, 1706–1710.
- 70 Lammers, S. and Meuwly, M. (2007) Investigating the relationship between infrared spectra of shared protons in different chemical environments: A comparison of protonated diglyme and protonated water dimer. *Journal of Physical Chemistry A*, **111**, 1638–1647.
- 71 Huang, S., Braams, B.J. and Bowman, J.M. (2005) Ab initio potential energy and dipole moment surfaces for H₅O₂⁺. *Journal of Chemical Physics*, **122**, 044308.
- 72 Asada, T., Haraguchi, H. and Kitaura, K. (2001) Simulation studies of proton transfer in N₂H₇⁺ cluster by classical ab initio Monte Carlo and quantum wave packet dynamics. *Journal of Physical Chemistry A*, **105**, 7423–7428.
- 73 Li, G.-S., Costa, M.T.C.M., Millot, C. and Ruiz-Lopez, M.F. (1999) Effect of solvent fluctuations on proton transfer dynamics: a hybrid AM1/MM molecular dynamics simulation on the [H₃N–H–NH₃]⁺ system. *Chemical Physics*, **240**, 93–99.

- 74 Wang, Y. and Gunn, J.R. (1999) Computational study of structures and proton transfer in hydrogen-bonded ammonia complexes using semiempirical valence-bond approach. *International Journal of Quantum Chemistry*, **73**, 357–367.
- 75 Meuwly, M. and Karplus, M. (2002) Simulation of proton transfer along ammonia wires: An ab initio and semiempirical density functional comparison of potentials and classical molecular dynamics. *Journal of Chemical Physics*, **116**, 2572–2585.
- 76 Clement, F. and Ford, I.J. (1999) Gas-to-particle conversion in the atmosphere: I. Evidence from empirical atmospheric aerosols. *Atmospheric Environment – Part A*, **33**, 1352.
- 77 Larson, L.J., Kuno, M. and Tao, F.M. (2000) Hydrolysis of sulfur trioxide to form sulfuric acid in small water clusters. *Journal of Chemical Physics*, **112**, 8830–8838.
- 78 Donaldson, D., Frost, G., Rosenlof, K. *et al.* (1997) Atmospheric radical production by excitation of vibrational overtones via absorption of visible light. *Geophysical Research Letters*, **24**, 2651–2654.
- 79 Vaida, V., Kjaergaard, H.G., Hintze, P.E. and Donaldson, D.J. (2003) Photolysis of sulfuric acid vapor by visible solar radiation. *Science*, **299**, 1566–1568.
- 80 Miller, Y. and Gerber, R.B. (2006) Dynamics of vibrational overtone excitations of H₂SO₄, H₂SO₄-H₂O: Hydrogen-hopping and photodissociation processes. *Journal of the American Chemical Society*, **128**, 9594–9595.
- 81 Nguyen, P.N. and Stock, G. (2003) Nonequilibrium molecular-dynamics study of the vibrational energy relaxation of peptides in water. *Journal of Chemical Physics*, **119**, 11350–11358.
- 82 Baughcum, S.L., Duerst, R.W., Rowe, W.F. *et al.* (1981) Microwave spectroscopic study of malonaldehyde (3-hydroxy-2-propenal). 2. Structure, dipole-moment, and tunneling. *Journal of the American Chemical Society*, **103**, 6296–6303.
- 83 Firth, D.W., Beyer, K., Dvorak, M.A. *et al.* (1991) Tunable far infrared spectroscopy of malonaldehyde. *Journal of Chemical Physics*, **94**, 1812–1819.
- 84 Smith, Z. and Wilson, E.B. (1983) The infrared spectrum of gaseous malonaldehyde (3-hydroxy-2-propenal). *Spectrochimica Acta Part A*, **39**, 1117–1129.
- 85 Firth, D.W., Barbara, P.F. and Trommsdorf, H.P. (1989) Matrix induced localization of proton tunneling in malonaldehyde. *Chemical Physics*, **136**, 349–360.
- 86 Chiavassa, T., Roubin, R., Piazzala, L. *et al.* (1992) Experimental and theoretical-studies of malonaldehyde – vibrational analysis of a strongly intramolecularly hydrogen-bonded compound. *Journal of Physical Chemistry*, **96**, 10659–10665.
- 87 Duan, C. and Luckhaus, D. (2004) High resolution IR-diode laser jet spectroscopy of malonaldehyde. *Chemical Physics Letters*, **391**, 129–133.
- 88 Yang, Y. and Meuwly, M. (2010) A generalized reactive force field for nonlinear hydrogen bonds: Hydrogen dynamics and transfer in malonaldehyde. *Journal of Chemical Physics*, **133**, 064503.
- 89 Baughcum, S.L., Smith, Z., Wilsom, E.B. and Duerst, R.W. (1984) Microwave spectroscopic study of malonaldehyde. 3. Vibration-rotation interaction and one-dimensional model for proton tunneling. *Journal of the American Chemical Society*, **106**, 2260.
- 90 Huang, J., Buchowiecki, M., Nagy, T. *et al.* (2014) Kinetic isotope effect in malonaldehyde from path integral Monte Carlo simulations. *Physical Chemistry Chemical Physics*, **16**, 204–211.

- 91 Johnson, M.R., Jones, N.H., Geis, A. *et al.* (2002) Structure and dynamics of the keto and enol forms of acetylacetone in the solid state. *Journal of Chemical Physics*, **116**, 5694–5700.
- 92 Lowrey, A.H., George, C., D’Antonio, P. and Karle, J. (1971) Structure of acetylacetone by electron diffraction. *Journal of the American Chemical Society*, **93**, 6399–6403.
- 93 Andreassen, A.L. and Bauer, S.H. (1972) Structures of acetylacetone, trifluoroacetylacetone, and trifluoroacetone. *Journal of Molecular Structure*, **12**, 381–403.
- 94 Srinivasan, R., Feenstra, J.S., Park, S.T. *et al.* (2004) Direct determination of hydrogen-bonded structures in resonant and tautomeric reactions using ultrafast electron diffraction. *Journal of the American Chemical Society*, **126**, 2266–2267.
- 95 Iijima, K., Ohnogi, A. and Shibata, S. (1987) The molecular structure of acetylacetone as studied by gas-phase electron diffraction. *Journal of Molecular Structure*, **156**, 111–118.
- 96 Caminati, W. and Grabow, J.U. (2006) The C_{2v} structure of enolic acetylacetone. *Journal of the American Chemical Society*, **128**, 854–857.
- 97 Howard, D., Kjaergaard, H., Huang, J. *et al.* (2015) Infrared and near infrared spectroscopy of acetylacetone and hexafluoroacetylacetone. *Journal of Physical Chemistry A*, **119** (29), 7980–7990.
- 98 Austin, R.H., Beeson, K.W., Eisenstein, L. *et al.* (1975) Dynamics of ligand-binding to myoglobin. *Biochemistry*, **14**, 5355–5373.
- 99 Kim, S., Jin, G. and Lim, M. (2004) Dynamics of geminate recombination of NO with myoglobin in aqueous solution probed by femtosecond mid-IR spectroscopy. *Journal of Physical Chemistry B*, **108**, 20366–20375.
- 100 Petrich, J.W., Lambry, J.C., Kuczera, K. *et al.* (1991) Ligand binding and protein relaxation in heme proteins: A room temperature analysis of NO geminate recombination. *Biochemistry*, **30**, 3975–3987.
- 101 Ouellet, H., Ouellet, Y., Richard, C. *et al.* (2002) Truncated hemoglobin HbN protects *Mycobacterium bovis* from nitric oxide. *Proceedings of the National Academy of Sciences USA*, **99**, 5902–5907.
- 102 Milani, M., Pesce, A., Ouellet, Y. *et al.* (2004) Heme-ligand tunneling in Group I truncated hemoglobins. *Journal of Biological Chemistry*, **279**, 21520–21525.
- 103 Bourassa, J.L., Ives, E.L., Marqueling, A.L. *et al.* (2001) Myoglobin catalyzes its own nitration. *Journal of the American Chemical Society*, **123**, 5142–5143.
- 104 Blomberg, L.M., Blomberg, M.R.A. and Siegbahn, P.E.M. (2004) A theoretical study of myoglobin working as a nitric oxide scavenger. *Journal of Biological Inorganic Chemistry*, **9**, 923–935.
- 105 Herold, S., Exner, M. and Nauser, T. (2001) Kinetic and mechanistic studies of the NO-mediated oxidation of oxymyoglobin and oxyhemoglobin. *Biochemistry*, **40**, 3385–3395.
- 106 Herold, S. (1999) Kinetic and spectroscopic characterization of an intermediate peroxynitrite complex in the nitrogen monoxide induced oxidation of oxyhemoglobin. *FEBS Letters*, **443**, 81–84.
- 107 Soloviov, M. and Meuwly, M. (2015) Reproducing kernel potential energy surfaces in biomolecular simulations: Nitric oxide binding to myoglobin. *Journal of Chemical Physics*, **143** (10), 105103.

